J. Fluid Mech. (1967), *vol.* 27, *part* 2, *pp.* 305–314
Printed in Great Britain

Shock-wave strengthening by area convergence

By DAVID A. RUSSELL
Jet Propulsion Laboratory, California Institute of Technology, Pasadena, California

(Received 6 May 1966)

A 17 in. diameter shock tube was coupled to a 1 in. tube by a 10° half-angle conical convergence. Timing measurements showed that the shock waves emerged from the convergence at 2–3 times their entrance speeds, and then decelerated downstream. After the application of a viscous correction, the shock speeds at the convergence exit agreed to within 5 % with equilibrium real-gas calculations of the model of Chester (1954), Chisnell (1957) and Whitham (1958). The downstream deceleration, due to viscosity and to higher-order interactions not included in the theory, was also briefly studied.

1. Introduction

A decrease in the cross-sectional area of a duct will result in an increase in the strength of a transmitted shock wave. The theoretical strengthening for an ideal gas is shown on figure 1 as a function of the area ratio, A_0/A_s, the ratio of specific heats of the test gas, γ, and the initial shock Mach number M_0. The lower set of curves was obtained from the model of Laporte (1954) which treats the convergence as an instantaneous area change. This solution is expected to be asymptotically valid far downstream of a region of varying area. The upper curves are from the non-steady one-dimensional theory of Chester (1954), Chisnell (1957) and Whitham (1958). This theory relates the shock strength directly to the cross-sectional area at the shock location, and it should be valid within a region of monotonically decreasing area. Barring two-dimensional and viscous effects, a shock wave is expected to emerge from a monotonic area convergence at a speed given by the non-steady theory, and then attenuate due to weak reflected disturbances until it reaches the asymptotic solution. Figure 1 shows that a large difference can exist between the two solutions for the shock speed, particularly for large convergence ratios.

Among the earliest experimental studies of shock strengthening by area convergence was the work of Hertzberg & Kantrowitz (1950), who were concerned with the applicability of the one-dimensional characteristics solution for the shock-wave motion. Kahane, Warren, Griffith & Marion (1954) made interferometric studies of the density field within a convergence. Blackman (1956) employed a converging channel of area ratio 34 : 1 to double the shock speed for studies of vibrational relaxation. Of particular interest is the work of Bird (1959), who measured the exit shock speed from various convergences and found a dependence on the convergence shape. For shallow-angle convergences, however, the shock speed was found to be close to that predicted by the non-steady theory.

Recently, Lee & Lee (1965) reported that pressure measurements made behind imploding cylindrical detonation-waves agreed with calculations based on the non-steady theory.

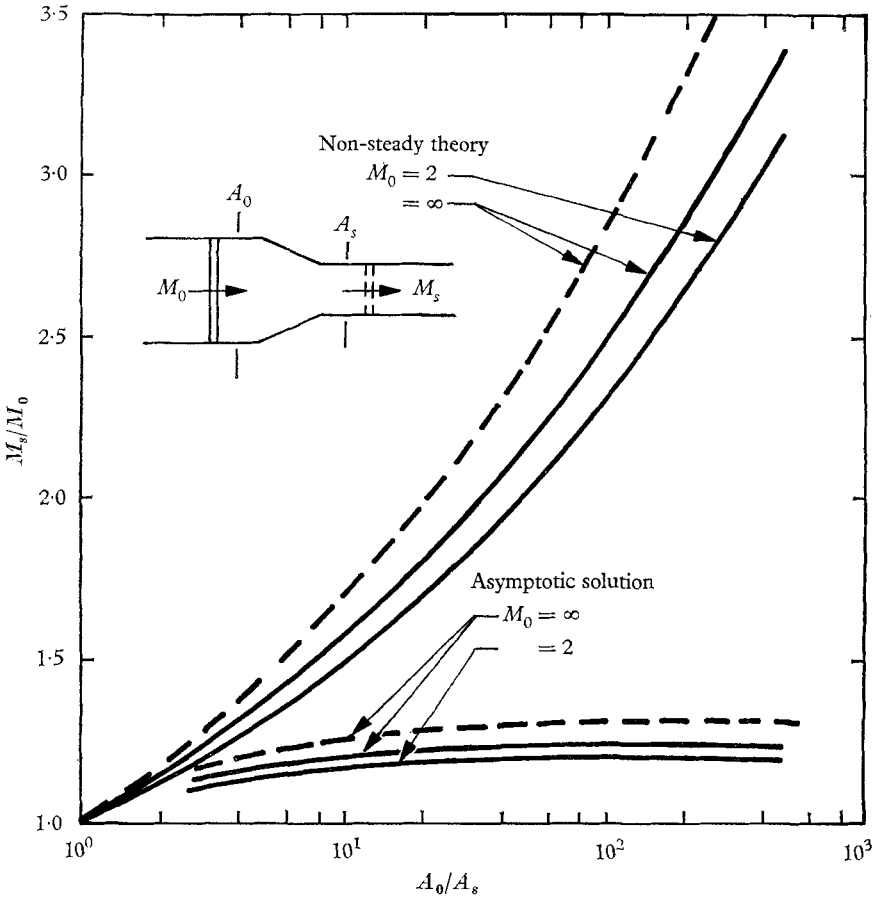

FIGURE 1. Theoretical strengthening (ideal gas). ——, $\gamma = \frac{7}{5}$; – – –, $\gamma = \frac{5}{3}$.

The present work extends these studies through observations of the shock-wave motion downstream of a large area-ratio convergence. The exit shock speed and the subsequent decay are examined for conditions which include significant real gas and viscous effects.

2. Experiment

A 17 in. shock tube (Liepmann, Roshko, Coles & Sturtevant 1962) was coupled by a 10° half-angle cone to a 1 in. diameter tube, providing an area convergence of 292 (see figure 2). Helium drivers were used with air as the usual test gas (a few runs were made with argon test gases). The length of the test-gas slug (Roshko & Smith 1964) at the entrance to the convergence always exceeded 1·5 times the convergence length, and it can be shown that disturbances reflected off the contact surface did not have time to catch the shock wave during the experiment.

The minimum length of laminar boundary layer behind the shock, obtained from the output of the thin-film gauges, was found to exceed a quarter of the convergence length.

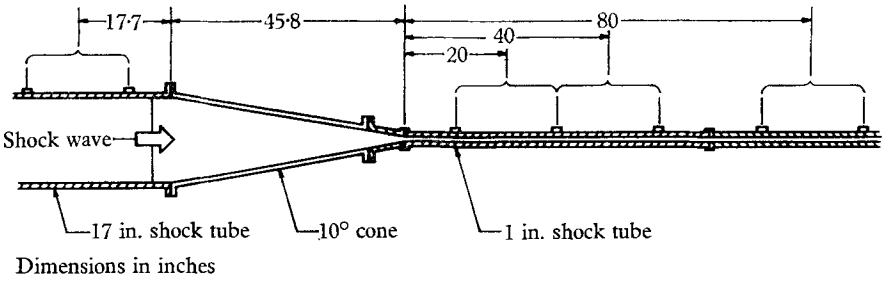

FIGURE 2. Scale drawing of the experiment. (The mid-point of each pair of gauges is indicated.)

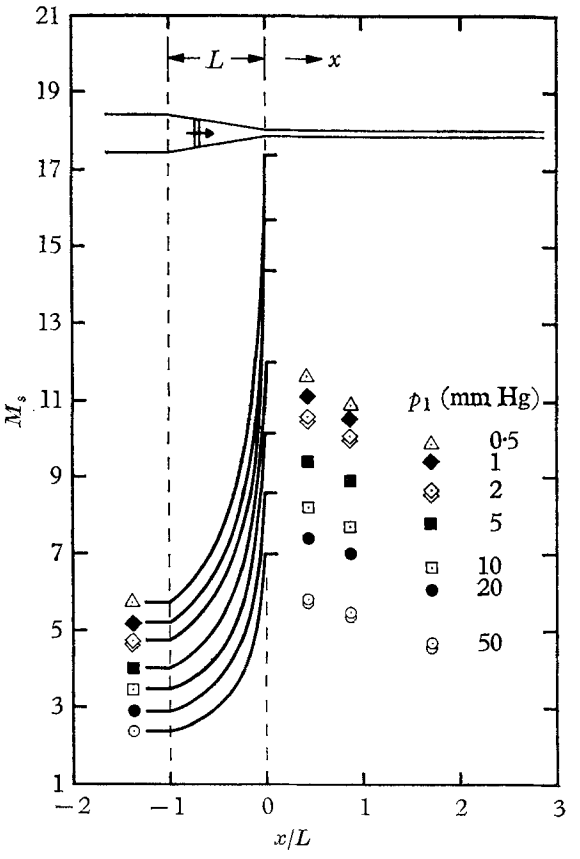

FIGURE 3. Measured shock motion in air for various values of the initial pressure. The solid lines are the non-steady theory for *ideal* air.

Pairs of thin-film gauges were used to time the average speed of the shock wave entering the convergence, and at three positions downstream. The individual gauges were spaced 20 in. apart, with the centre of each pair located as shown on figure 2. The data are presented on figure 3, where the shock Mach number M_s

(the shock speed divided by the speed of sound in the undisturbed gas) is plotted against the downstream position of the centre of each gauge pair, measured in units of the convergence length. Each run is indicated by a different symbol, corresponding to a different value of the initial pressure p_1, and entering shock Mach number M_0. The high degree of repeatability of the shock-wave motion is illustrated by duplicate runs with p_1 equal to 50 and 2 mm Hg. The data show that the shock Mach number is more than doubled by the convergence, and that it decays with distance downstream.

The ideal non-steady shock history is indicated for each run by a solid curve on figure 3. The experimental results can be compared with the ideal theory by extrapolating the data back to the convergence exit. When this is done, it is found that the agreement gets progressively worse as M_0 is raised and p_1 lowered. This is due to the onset of real-gas effects, as well as the viscous attenuation encountered at the low p_1 used to obtain the higher values of M_0. These effects must be understood before the data can be interpreted further.

3. Correction procedures

3.1. *Non-steady theory for real gases*

In appendix 1, it is shown that the convergence area-ratio is related to the shock Mach number by

$$\frac{A_s}{A_0} = \exp\left\{\int_{M_0}^{M_s} g\, dM_s\right\},$$

where the subscript 0 refers to the initial conditions. g is plotted on figure 4. Real-gas effects are seen to increase the value of g, and hence reduce M_s for a given A_0/A_s and M_0. Specific calculations were made for the experimental conditions of figure 3 and are shown as the solid lines on figure 6. A comparison of the two figures will show that the real-gas solutions reduced the expected exit M_s by 5–20 %.

3.2. *Effects of viscosity*

An attempt was made to correct for the effects of viscosity by varying the pressure for a series of otherwise identical runs. This was not successful, principally because of the changing laminar-turbulent nature of the boundary layer with pressure level. It was therefore necessary to develop an analytical correction procedure, assuming that viscous effects are small and are superimposed on the wave effects.

Boundary-layer corrections were expected to be significant only in the constricted downstream tube. For the calculation of the viscous correction, a shock wave and contact surface were assumed to originate near the entrance to this tube, and the laminar boundary layer extending between them was used to estimate the viscous attenuation of the shock. The calculation is described in appendix 2; the resulting attenuation parameter, C, is shown on figure 5. Note that figure 5 is for real gases; ideal-gas calculations were found to give larger values of C by a factor that approached an order of magnitude at high M_s.

M_s for each point on figure 3 was corrected by ΔM_s estimated from figure 5, arbitrarily taking the length as that measured from the entrance of the con-

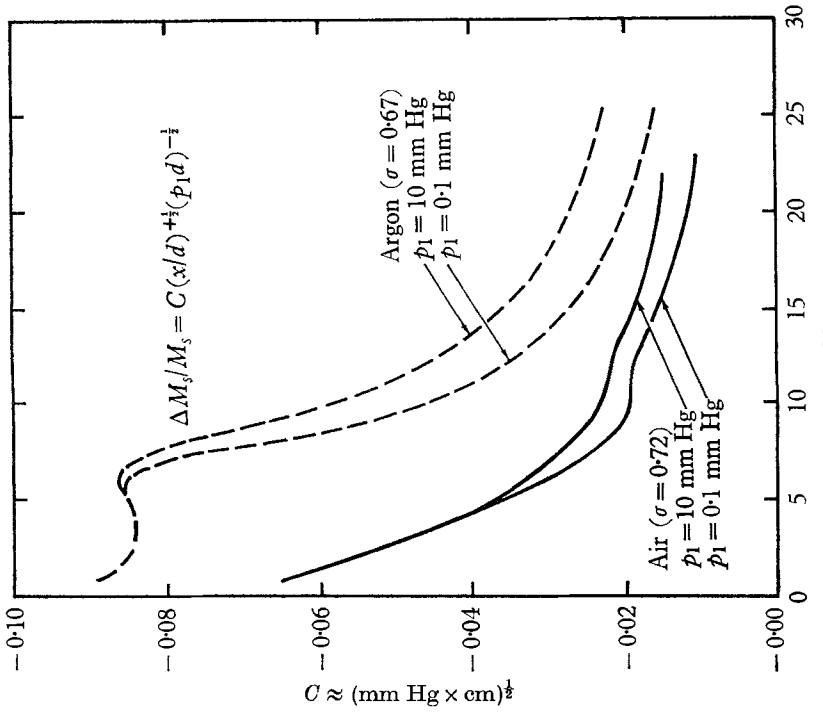

FIGURE 5. Viscous attenuation due to laminar shock boundary-layer in a constant-area tube. Equilibrium real-gas solutions with variable $\rho\mu$. $T_1 = 300$ °K.

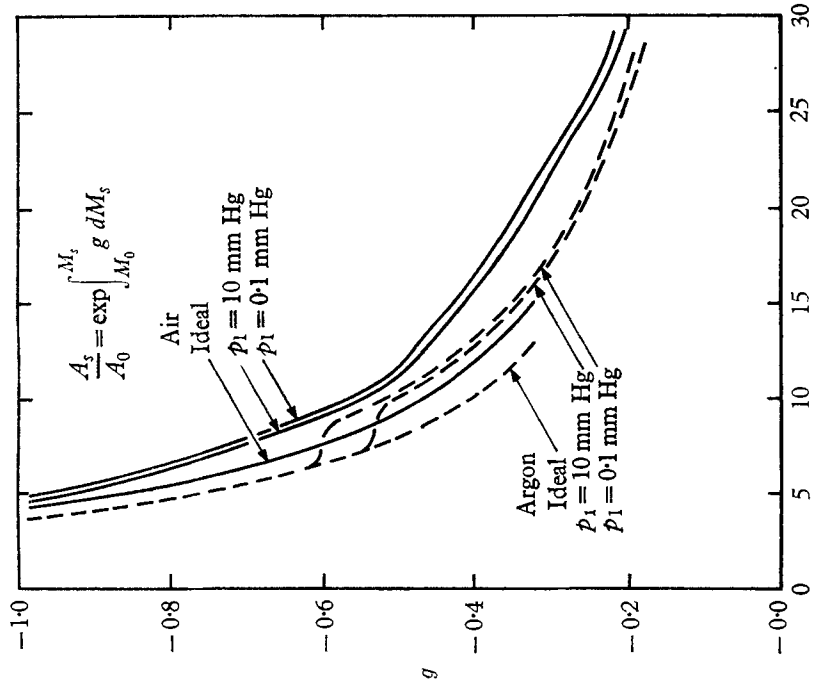

FIGURE 4. Shock strengthening parameter g.

vergence. This resulted in a maximum correction of slightly greater than 20 %. While the correction model is certainly not precise, it is simple and correlates the data satisfactorily.

4. Results and discussion

The corrected data are compared with the non-steady theory for real air on figure 6. Since there was no way of making a precise local measurement, it was necessary to extrapolate the data in order to find M_s at the convergence exit. The

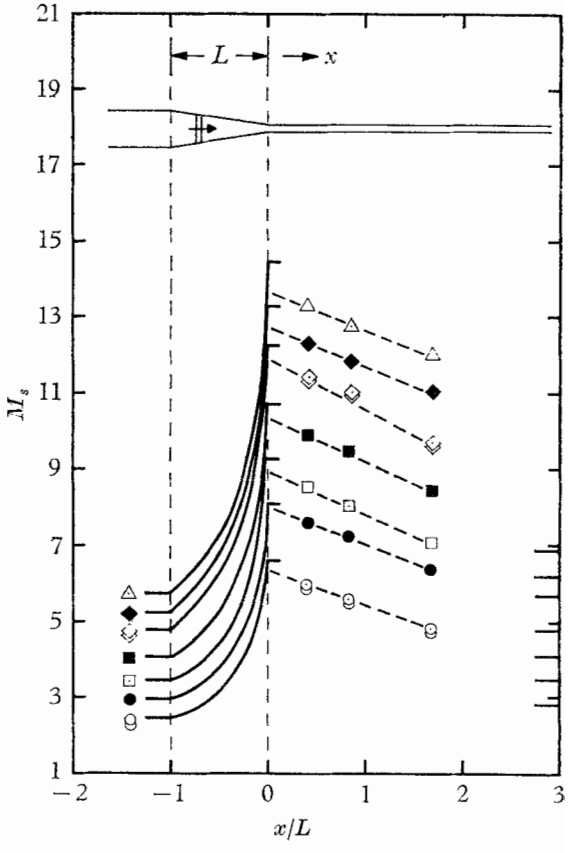

FIGURE 6. Corrected data compared with the non-steady theory for *real* air. The bars on the right border are the asymptotic solutions.

straight lines on figure 6 indicate that the exit M_s reached 95–100 % of the predicted values. Considering the accuracy of the correction and extrapolation procedures, this is a satisfactory agreement with the non-steady theory. The results demonstrate the substantial increase in shock Mach number that can be obtained through the use of area convergence.

Once the shock wave has left the convergence, weak reflected waves are expected to attenuate it to the asymptotic solution. This limiting solution is indicated by the bars on the right border of figure 6. The data show that it should take a distance of 4–6 convergence lengths to complete the decay. The decay

length should be insensitive to the overall M_s level, since it is readily shown that the ratio of the closing speed of weak waves to the shock speed is a weak function of M_s.

The effect of changing γ was investigated with runs using an argon test gas. Good agreement with the non-steady calculations was again observed for the exit M_s, and the decay rate was similar to that of figure 6. The effect of varying

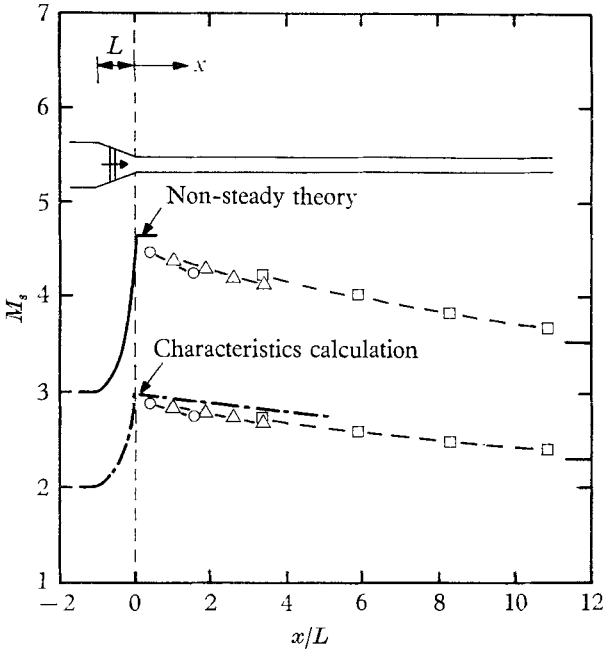

FIGURE 7. Corrected air data, 1961 experiments. $A_0/A_s = 10$ with convergence half-angles of 5, 10 and 30°. The bars on the right border are the asymptotic solutions. ○, 5°; △, 10°; □, 30°.

the convergence angle was studied earlier (Russell 1961), using a smaller shock tube with convergence area ratios of 10 and 4. Some of the results, corrected for viscous effects, are presented on figure 7. Here it is seen that the downstream shock history depended primarily on the normalized downstream distance and not on the convergence angle. This suggests that two-dimensional effects are of limited importance, at least for half-angles under 30°. Indeed, the $M_0 = 2$ shock history showed reasonable agreement with a one-dimensional characteristics calculation (see figure 7).

It is beyond the scope of this study to discuss the time variation of a flow property at a fixed location. However, it is interesting to note that the non-viscous contribution to the time variation should scale inversely with the convergence length. Further, from the acceleration histories of figures 3, 6 and 7, much lower gradients would be expected in the flow a short distance downstream of the convergence than in the convergence itself.

The author would like to thank Prof. H. W Liepmann and his associates at the Graduate Aeronautical Laboratories of the California Institute of Technology

for the use of the GALCIT 17 in. shock tube. Valuable discussions with Prof. Anatol Roshko (who suggested the problem) are gratefully acknowledged. This paper presents the results of one phase of research carried out at the Jet Propulsion Laboratory, California Institute of Technology, under Contract No. NAS 7–100, sponsored by the National Aeronautics and Space Administration.

Appendix 1. Non-steady theory for a real gas

The one-dimensional equations for the flow behind the shock wave are (Whitham 1958; Spence & Woods 1964):

$$\left.\begin{aligned} \frac{\partial \rho}{\partial t}+\frac{\partial}{\partial x}(\rho u) &= m, \\ \rho\frac{\partial u}{\partial t}+\rho u\frac{\partial u}{\partial x}+\frac{\partial p}{\partial x} &= 0, \\ \left(\frac{\partial}{\partial t}+u\frac{\partial u}{\partial x}\right)\ln\left(\frac{p}{\rho^{\gamma}}\right) &= 0, \end{aligned}\right\} \tag{A 1}$$

where $m = -(\rho u)/A\, dA/dx$, the mass adjustment term due to the changing cross-sectional area. The last equation is a statement of particle isentropy. After it has been used to eliminate the density derivatives, adding and subtracting the first two equations results in

$$\left[\frac{\partial}{\partial t}+(u\pm a)\frac{\partial}{\partial x}\right]p \pm \rho a\left[\frac{\partial}{\partial t}+(u\pm a)\frac{\partial}{\partial x}\right]u = ma^2.$$

Defining the variables

$$\eta = x-(u+a)t \quad \text{and} \quad \xi = x-(u-a)t,$$

the equations become,

$$\text{along} \quad d\eta = 0: \quad dp+\rho a\, du = \tfrac{1}{2}ma\, d\xi = \frac{\rho u a^2}{u+a}\frac{dA}{A}, \tag{A 2a}$$

$$\text{along} \quad d\xi = 0: \quad dp-\rho a\, du = -\tfrac{1}{2}ma\, d\eta = -\frac{\rho u a^2}{u-a}\frac{dA}{A}. \tag{A 2b}$$

Put $p = p_2+p'$, etc., and integrate for small perturbations. Adding and subtracting then produces

$$\rho_2 a_2(u-u_2) = F(\eta)+G(\xi)+\frac{\rho_2 a_2^3 u_2}{u_2^2-a_2^2}\frac{A(x)-A_2}{A_2},$$

$$p-p_2 = F(\eta)-G(\xi)-\frac{\rho_2 a_2^2 u_2^2}{u_2^2-a_2^2}\frac{A(x)-A_2}{A_2}.$$

Here subscript 2 refers to the unperturbed conditions. $F(\eta)$ and $G(\xi)$ are constants of integration that must be evaluated from the boundary conditions. Now Whitham's rule (Whitham 1958) amounts to setting $F(\eta)$, representing re-reflected disturbances overtaking the shock wave from behind, identically equal to zero. $F(\eta)$ arises from the integration of (A 2a); if it is equal to zero, this equation must apply for the complete flow and not just on lines of η = const. Applying (A 2a) at the shock wave, again for small perturbations,

$$\left[p_1\frac{d(p_2/p_1)}{dM_s}+\rho_2 a_2 a_1\frac{d(u_2/a_1)}{dM_s}\right]dM_s = -\rho_2 a_2^2\left[\frac{u_2/a_1}{u_2/a_1+a_2/a_1}\right]\frac{dA}{A}.$$

After integration:
$$\frac{A_s}{A_0} = \exp \int_{M_0}^{M_s} g\, dM_s, \tag{A 3}$$

where
$$g = -\left[\frac{1}{\gamma_1}\frac{d(p_2/p_1)}{dM_s} + \frac{\rho_2}{\rho_1}\frac{a_2}{a_1}\frac{d(u_2/a_1)}{dM_s}\right]\left[\frac{\rho_2}{\rho_1}\left(\frac{a_2}{a_1}\right)^2\left(\frac{u_2/a_1}{u_2/a_1 + a_2/a_1}\right)\right]^{-1}.$$

Here A_0 and M_0 refer to the unperturbed area and shock Mach number, respectively. p_2, ρ_2, etc., refer to the unperturbed flow quantities immediately behind a shock wave whose shock Mach number is M_s; p_1, ρ_1, etc., to the gas that the shock wave is travelling into. g has been calculated for air and argon, using both ideal gas and equilibrium real-gas assumptions. The results are presented on figure 4.

Appendix 2. Viscous attenuation

In order to find the viscous attenuation in a tube of uniform cross-sectional area, (A 1) are first written for the core flow, where now
$$m = -4\rho_2 \frac{(U_s - u_2)}{d}\frac{d\delta^*}{d(U_s t - x)},$$
representing the mass-loss term due to the boundary layer. m has been expressed in shock-fixed co-ordinates, where $U_s t - x$ is the distance from the shock, and δ^* the boundary-layer displacement thickness. Assuming laminar boundary layers, define the constant K so that
$$\delta^* = -K\left[\frac{\nu_w (U_s t - x)}{U_s - u_2}\right]^{\frac{1}{2}};$$
thus
$$m = -\frac{2K\rho_2 (U_s - u_2)}{d}\left[\frac{\nu_w}{(U_s - u_2)(U_s t - x)}\right]^{\frac{1}{2}}.$$

Here ν_w is the kinematic viscosity evaluated at the wall.

Following the same procedure as in appendix 1 yields
$$\rho_2 a_2 (u - u_2) = -\frac{4K\rho_2 a_2^2}{d}\frac{(U_s - u_2)}{(U_s - u_2)^2 - a_2^2}\left[\frac{\nu_w (U_s t - x)}{U_s - u_2}\right]^{\frac{1}{2}} + F\left(\frac{\eta}{(U_s - u_2) - a_2}\right) - g\left(\frac{\xi}{(U_s - u_2) + a_2}\right),$$
$$p - p_2 = -\frac{4K\rho_2 a_2^2}{d}\frac{(U_s - u_2)^2}{(U_s - u_2)^2 - a_2^2}\left[\frac{\nu_w (U_s t - x)}{U_s - u_2}\right]^{\frac{1}{2}} + F\left(\frac{\eta}{(U_s - u_2) - a_2}\right) + g\left(\frac{\xi}{(U_s - u_2) + a_2}\right). \tag{A 4}$$

The unknown functions f and g must be evaluated from the boundary conditions. One boundary condition is that the perturbed pressure and velocity must be related to the shock Mach-number perturbation by the shock relations applied at the unperturbed position, $x = U_s t$. The other will be taken to be that the perturbations are zero along some imaginary contact surface whose unperturbed position is given by $x = u_2 t$. This is equivalent to matching acoustic impedances with identical gas on both sides of the interface. Boundary conditions appropriate to the normal shock-tube situation are discussed by Spence & Woods (1964).

Evaluation of the unknown functions in (A 4) ultimately results in the shock Mach-number perturbation in a real gas:

$$\frac{\Delta M_s}{M_s} = C\left(\frac{x}{d}\right)^{\frac{1}{2}} (p_1 d)^{-\frac{1}{2}}, \tag{A 5}$$

where $$C = \frac{-4KM^*}{M_s(1-M^*)^{\frac{1}{2}}}\left[\frac{1}{\gamma_1}\frac{d(p_2/p_1)}{dM_s} + \frac{\rho_2}{\rho_1}\frac{a_2}{a_1}\frac{d(u_2/a_1)}{dM_s}\right]^{-1}\frac{\rho_2}{\rho_1}\left(\frac{a_2}{a_1}\right)^2\left(\frac{\nu_w}{U_s d}\right)^{\frac{1}{2}}.$$

Here $M^* = (U_s - u_2)/a_2$. Note the similarity between C and g of appendix 1. C has been calculated for real gases with the laminar boundary-layer solutions of Mirels (1966). It is shown on figure 5.

REFERENCES

Bird, G. A. 1959 *J. Fluid Mech.* **5**, 60.

Blackman, V. 1956 *J. Fluid Mech.* **1**, 61.

Chester, W. 1954 *Phil. Mag.* **7**, 45, 1293.

Chisnell, R. F. 1957 *J. Fluid Mech.* **2**, 286.

Hertzberg, A. & Kantrowitz, A. 1950 *J. Appl. Phys.* **21**, 874.

Kahane, A., Warren, W. R., Griffith, W. C. & Marion, A. A. 1954 *J. Aero. Sci.* **21**, 505.

Laporte, O. 1954 *Los Alamos Scientific Laboratory Rept.* no. LA-1740.

Lee, J. H. & Lee, B. H. K. 1965 *Phys. Fluids*, **8**, 2148.

Liepmann, H. W., Roshko, A., Coles, D. & Sturtevant, B. 1962 *Rev. Sci. Instr.* **33**, 625.

Mirels, H. 1966 *Phys. Fluids*, **9**, 1265.

Roshko, A. & Smith, J. A. 1964 *AIAA J.* **2**, 186.

Russell, D. A. 1961 Ph.D. Thesis (Part III), California Institute of Technology.

Spence, D. A. & Woods, B. A. 1964 *J. Fluid Mech.* **19**, 161.

Whitham, G. B. 1958 *J. Fluid Mech.* **4**, 337.